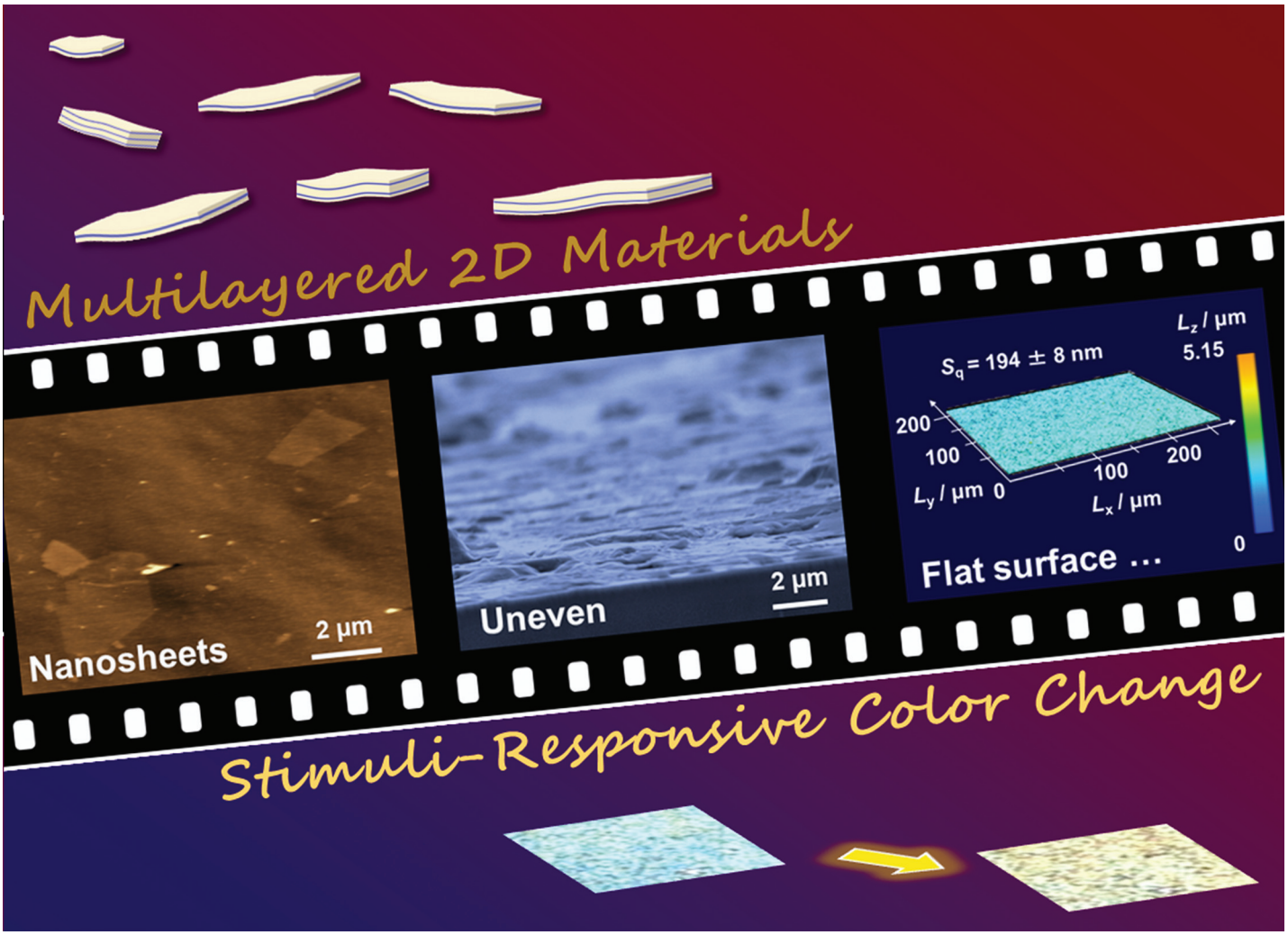

Showcasing research from Professor Yuya Oaki's group at the Department of Applied Chemistry, Faculty of Science and Technology, Kaio University, Japan.

Stimuli-responsive noniridescent structural color of thin-film coating based on multilayered nanosheets preserving interlayer space

This paper shows new architectonics for applications of multilayered 2D materials. Exfoliated nanosheets preserving multilayered structures exhibit both the intercalation and building-block capabilities. Stimuli-responsive thin-film coating with noniridescent structural color is prepared using the exfoliated nanosheets with the multilayered structures.

Image reproduced by permission of Yuya Oaki from *Nanoscale*, 2026, **18**, 10085.

As featured in:

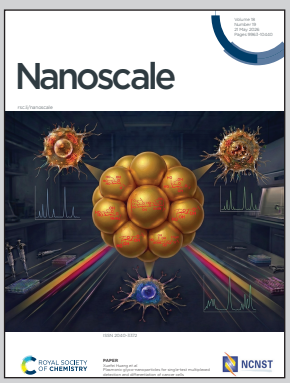

See Yuya Oaki *et al.*, *Nanoscale*, 2026, **18**, 10085.

ROYAL SOCIETY OF CHEMISTRY

rsc.li/nanoscale

Registered charity number: 207890

Nanoscale

PAPER

View Article Online
View Journal | View Issue

Cite this: *Nanoscale*, 2026, **18**, 10085

Stimuli-responsive noniridescent structural color of a thin-film coating based on multilayered nanosheets preserving the interlayer space

Yuka Kitamura,[a] Hisafumi Sudo,[a] Hiroaki Imai,[a] Yui Maejima,[b] Michinari Kohri[b] and Yuya Oaki*[a]

Received 16th December 2025,
Accepted 11th February 2026

DOI: 10.1039/d5nr05285h

rsc.li/nanoscale

Two-dimensional (2D) anisotropic structures have numerous advantages for designing functional materials. Layered materials accommodate guests in their interlayer space, and exfoliated nanosheets are used as units to obtain organized architectures. If exfoliated nanosheets preserving their multilayered structures are prepared, both the intercalation and building-block capabilities can be used for functionalization. In the present work, a stimuli-responsive thin-film coating with noniridescent structural color was prepared using exfoliated nanosheets with multilayered structures. The precursor layered composite of a host transition-metal oxide and a guest organic molecule was exfoliated into surface-modified nanosheets. The resultant nanosheet was not a monolayer but comprised multilayers with an interlayer space. Coating the exfoliated nanosheets provided a thin film with uneven thickness and noniridescent structural color. As additional guest molecules were introduced into the interlayer space of the multilayers in the nanosheet, an increase in the film thickness induced changes in the structural color. Harmful biogenic amines and their mixtures were colorimetrically quantified using the prepared thin-film sensor. The thin-film coating of the multilayered nanosheets has potential for a variety of sensing applications.

Introduction

Two-dimensional (2D) structures of layered materials and ultrathin nanosheets have attracted much research interest, regardless of their inorganic or organic nature.[1–16] Intercalation of guests is used for the assembly, storage, and transport of molecules and ions in the interlayer space.[17–21] Exfoliation of pristine layered materials provides anisotropic nanostructures, such as monolayered and few-layered nanosheets.[22–26] However, both the intercalation and exfoliation capabilities are not effectively used for functionalization because the interlayer space decreases with the exfoliation. In general, monolayered and/or few-layered nanosheets are selectively prepared by purification, followed by the removal of the thicker layers. Syntheses and applications of multilayered nanosheets have not yet been fully studied in previous works. In the present work, nanosheets preserving the interlayer space were synthesized by exfoliation of the precursor layered composites. A homogeneous noniridescent structural color was obtained by coating the exfoliated nanosheets (Fig. 1a and b). The interlayer space of the multilayered nanosheets was used for sensing with the intercalation of the additional guests (Fig. 1c and d). Results show the potential of the multilayered nanosheets, having both the anisotropic morphology and interlayer space, as a new nanoarchitectonics for 2D materials.

Nanosheets are generally synthesized in the liquid phase and then used in assembled states, such as thin-film coatings, liquid crystals, gels, and composites.[27–32] One of the promising applications of nanosheets is in the development of optical functional materials exhibiting structural colors. Liquid crystalline assemblies and stable colloidal dispersions were prepared by tuning the interactions between nanosheets.[33–37] Lotsch *et al.* developed one-dimensional photonic crystals (Blagg stacks) with stimuli-responsiveness.[38,39] The Blagg stacks were prepared by the layer-by-layer coating of the monolayered nanosheets and particles. As the stacked monolayers accommodated guest molecules, such as water and amines, the changes in the structural color were applied for sensing application. However, the structural colors were iridescent, *i.e.* angle dependent. Such iridescent structural color was observed on the flat coating of nanosheets.[39–43] The angle-independent structural color is preferred for practical sensing applications because the color would not change by the angle of view. In general, an appropriate inhomogeneity is required to achieve

[a]*Department of Applied Chemistry, Faculty of Science and Technology, Keio University, 3-14-1 Hiyoshi, Kohoku-ku, Yokohama 223-8522, Japan. E-mail: oakiyuya@applc.keio.ac.jp*
[b]*Department of Applied Chemistry and Biotechnology, Graduate School of Engineering, Chiba University, 1-33 Yayoi-cho, Inage-ku, Chiba 263-8522, Japan*

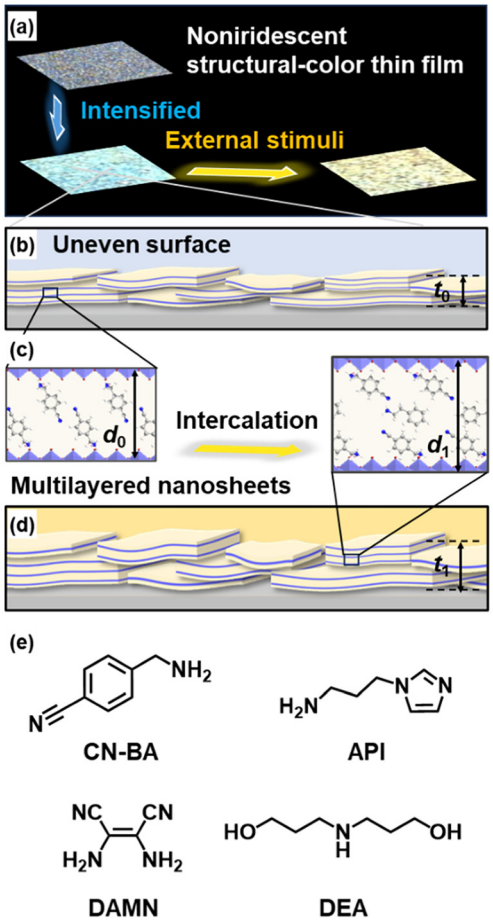

Fig. 1 Thin-film coating of the surface-modified multilayered nanosheets exhibiting noniridescent structural color. (a) Changes in the noniridescent structural color in response to external stimuli. (b) Uneven surface of the coating. (c) Interlayer space in the multilayered nanosheets with the intercalation capability of additional guests. (d) Increase in the film thickness with the expansion of the interlayer space. (e) Molecular structures of the biogenic amines as sensing targets.

the noniridescent structural color.[44,45] Angle-independent structural color was prepared by coating the nanosheets on the surfaces.[46–48] However, stimuli-responsive changes in the noniridescent color were not achieved in previous works. In the present work, coating the multilayered nanosheets provided the thin film exhibiting the noniridescent structural color. The color changes were observed in response to external stimuli (Fig. 1).

The dispersion state of the nanosheets has an impact on the coating. Our group has focused on the exfoliation of the layered composites based on host inorganic layers and organic guests.[49–55] In general, precursor layered materials are exfoliated in a dispersion medium. However, the selected dispersion medium is not always suitable for the subsequent coating. Our exfoliation method is able to synthesize the surface-modified nanosheets in a variety of polar and nonpolar organic media. For example, the surface-modified niobate nanosheets formed a thin film with an uneven surface morphology, exhibiting angle-independent structural color.[48] However, the intensity of the structural color was weak. The formation mechanisms were not elucidated to obtain the thin-film coating exhibiting noniridescent structural color. In the present work, the noniridescent structural color was enhanced by elucidation of the coating conditions and formation mechanisms. Moreover, the film was applied to colorimetric sensing of harmful biogenic amines. Biogenic amines, such as histamine and tyramine, are produced by the decomposition of proteins in foods and drinks.[56–58] When the concentration increases with deterioration, we are faced with the risk of foodborne illnesses. These small molecules are not easily detected using typical analytical methods because these amines have no chromophore for photochemical detection. The selective detection of these amines in the range of 10^{-8}–10^{-2} mol dm^{-3} was achieved by specifically designed sensing probes to recognize the targets (Fig. S1 in the SI). However, the health damage is caused not by the amount of each amine but by the total amount of the mixtures. Therefore, non-selective sensing of the total concentration is required. In the present work, the multilayered nanosheets accommodated these amines as additional guests in the interlayer space without selectivity.

Results and discussion

Syntheses of the surface-modified nanosheets with different sizes

Preparation and exfoliation of the precursor layered composites were carried out according to the methods employed in our previous works.[51–53] The detailed procedure is described in the SI. Four guest amines, such as 4-(aminomethyl)benzonitrile hydrochloride (CN-BA), 1-(3-aminopropyl)imidazole (API), diaminomaleonitrile (DAMN), and diethanolamine (DEA), were intercalated in the interlayer space of host layered niobate (Fig. 1e, Table 1, and Fig. S2 in the SI). The combinations of the guests and dispersion media were selected to control the thickness and lateral-size distribution of the nanosheets, as mentioned later. The structure of these precursor layered composites was characterized in our previous reports.[52,53] The layered composites were exfoliated into the nanosheets in the following dispersion media (Table 1): purified water for the CN-BA-, API-, and DAMN-intercalated niobates and ethanol for CN-BA- and DEA-intercalated niobate. The resultant dispersion liquid was filtered to purify by removing the bulky unexfoliated materials.

These guest-medium combinations for the exfoliation were selected based on the relationship between the lateral-size distribution and thickness.[53,55] Our previous study indicates that the thin and thick surface-modified nanosheets have polydispersed and monodispersed lateral sizes, respectively.[55] The machine-learning-based prediction model for the size distribution proposes potential guest-medium combinations forming monodispersed or polydispersed nanosheets.[53] Based on this fact and prediction, the thin nanosheets with polydispersed lateral size were synthesized by the exfoliation of

Table 1 Precursor layered composites based on niobate and their exfoliated nanosheets

Guests	d_0/nm	x/—[a]	y/—[a]	Ref.[b]	Dispersion media	Lateral size/nm	Thickness/nm
None (pristine layered niobate)	0.94	—	—	—	—	—	—
4-Cyanobenzylamine (CN-BA)	2.98	2.22	0.53	53	Water	286 ± 288	8.8 ± 4.2
					Ethanol	371 ± 551	9.4 ± 5.4
1-(3-Aminopropyl)imidazole (API)	2.15	2.79	0.95	53	Water	293 ± 259	11.3 ± 7.5
Diaminomaleonitrile (DAMN)	0.80	0.87	0.84	52	Water	115 ± 93.0	11.9 ± 5.8
Diethanolamine (DEA)	2.03	1.31	0.74	53	Ethanol	740 ± 546	12.3 ± 7.5

[a] x, y in $K_{4-x}(Guest)_xNb_6O_7{\cdot}yH_2O$. [b] Structural characterization of the precursor layered composites.

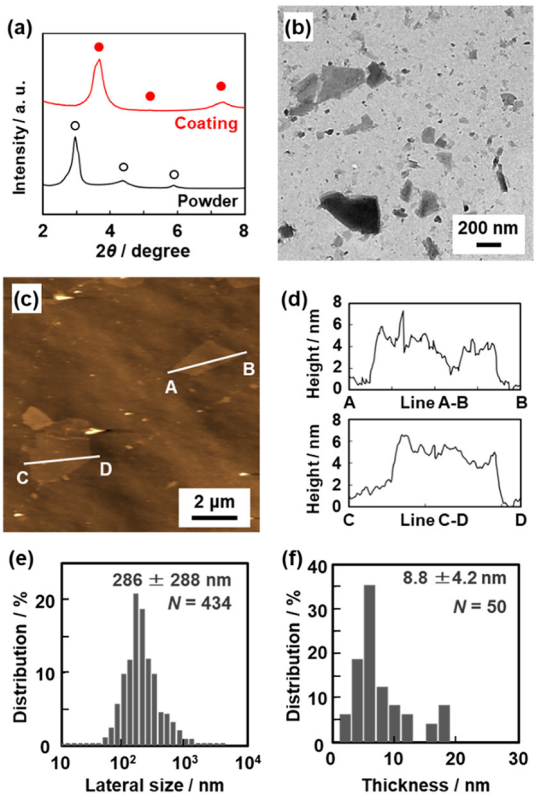

Fig. 2 Structural analysis of the layered CN-BA-niobate and its exfoliated nanosheets. (a) XRD patterns of the layered CN-BA-niobate powder (black) and its exfoliated nanosheets coated on a silicon substrate (red). (b) TEM image of the nanosheets. (c and d) AFM image of the nanosheets (c) and their height profiles (d). (e and f) Lateral-size (e) and height (f) distributions.

CN-BA-, API-, and DAMN-intercalated niobates in water. On the other hand, the exfoliation of CN-BA- and DEA-intercalated niobates was carried out in ethanol to synthesize thick nanosheets with monodispersed lateral size. Therefore, the present work focused on the effects of the sizes of nanosheets coating conditions on the morphologies of the thin films and their structural color.

The precursor CN-BA-intercalated niobate showed peaks characteristic of the layered structure corresponding to d_0/n (n = 1, 2, and 3) on the assumption of the interlayer distance (d_0) = 2.98 nm in the X-ray diffraction (XRD) pattern (the black profile in Fig. 2a). The original d_0 = 0.943 nm for the pristine niobate was increased with the intercalation of the guest. After exfoliation in purified water, the (CN-BA)-niobate nanosheets 286 ± 288 nm (the number of the counted samples (N) = 434) in lateral size were observed in transmission electron microscopy (TEM) images (Fig. 2b and e). The average thickness was 8.8 ± 4.2 nm (N = 50) in atomic force microscopy (AFM) images (Fig. 2c, d and f). Based on the thickness, both monolayers and multilayers were formed by the exfoliation. Table 1 summarizes the sizes of the nanosheets prepared by other guest-medium combinations (Fig. S2 in the SI). The nanosheets with different sizes were selectively prepared based on the prediction.

Coating of the surface-modified nanosheets

The coating conditions were optimized to obtain an intense non-iridescent structural color. Then, the different sizes of the nanosheets were used to study their effects on the coating behavior and structural color. The aqueous colloid containing the exfoliated CN-BA niobate nanosheets was dropped on a mirror-polished and cleaned silicon (Si) substrate (Fig. 3a). The substrate was heated to promote the evaporation of water. The photographs were taken on the stage of optical microscopy with the irradiation of white light. Although the bare Si substrate showed strong reflection (the left panel in Fig. 3a), a different color was observed after coating the nanosheets (the other panels in Fig. 3a). The intensity and homogeneity of the color were enhanced by changes in the coating conditions: concentration of the nanosheets (C_{ns}), volume of the dispersion liquid (V_{ns}), and temperature of the substrate (T_s). The noniridescent pale blue color was observed at the initial coating conditions, C_{ns} = 2.5 g dm^{-3}, T_s = 140 °C, and V_{ns} = 50 mm^3 (μL) (green frame, sample A in Fig. 3a).[48] The observed colors were analyzed and summarized in the chromaticity diagram with varying C_{ns}, T_s, and V_{ns} (Fig. S3 in the SI). The intense structural color was observed at higher C_{ns} (0.25–2.5 g dm^{-3}, (i) in Fig. 3a). The intensified color and homogeneous coating were achieved with rising T_s (100 °C–180 °C, (ii) in Fig. 3a) and decreasing V_{ns} (10–150 mm^3, (iii) in Fig. 3a). The homogeneous and noniridescent blue color was obtained at C_{ns} = 2.5 g dm^{-3}, T_s = 180 °C, and V_{ns} = 10 mm^3 (yellow frame, sample B in Fig. 3a). As the higher T_s promotes faster evaporation, the nanosheets are homogeneously deposited throughout the drop-casted area without aggregation. C_{ns} and V_{ns} are

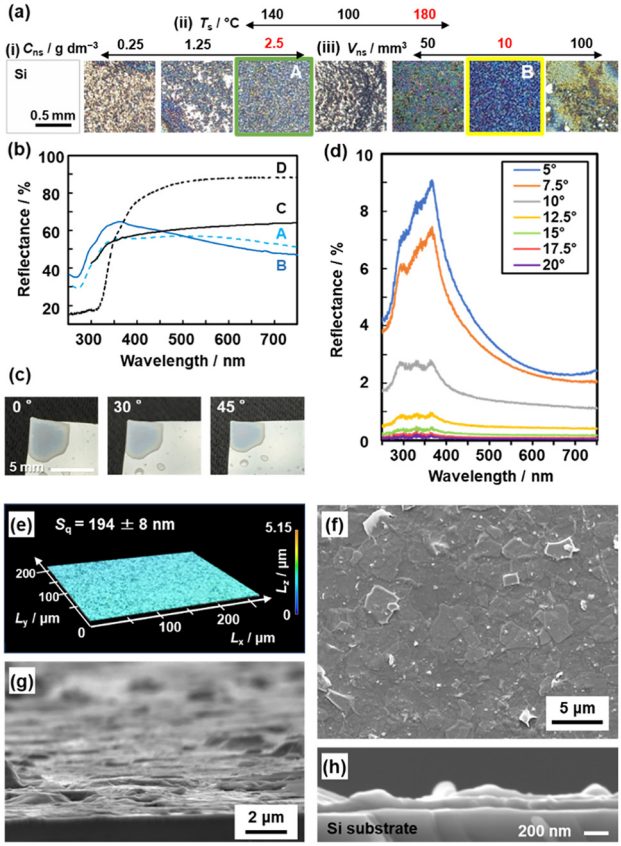

Fig. 3 Structure and morphology of the CN-BA-niobate nanosheet thin-film coatings exhibiting noniridescent structural color. (a) Optical microscopic images of the coatings on a cleaned silicon substrate (left) with changing C_{ns} (i), T_s (ii), and V_{ns} (iii). (b) UV-vis reflectance spectra of the nanosheet thin films exhibiting the structural color (samples A and B), the reference coating without structural color (sample C), and the powder of the layered CN-BA-niobate (sample D) measured by diffuse reflectance using an integrated sphere. (c and d) Photographs (c) and UV-vis reflectance spectra (d) of a thin film exhibiting the structural color (sample B) with changing $\theta_i = \theta_r$. (e) Laser microscopy image of sample B. (f–h) Surface (f), bird-view (g), and cross-sectioal (h) SEM imagess of the sample B.

related to the amount of the nanosheets sufficient for the homogeneous coating.

Optical properties of the noniridescent structural color

The structural color at the initial condition (sample A) was intensified after the optimization (sample B) (Fig. 3a). Two reference samples were prepared to compare the optical properties using UV-vis reflectance spectra: the coating with no structural color at C_{ns} = 2.5 g dm^{-3}, T_s = 80 °C, and V_{ns} = 50 mm^3 (sample C) and the pelletized powder of the precursor layered CN-BA niobate (sample D). The UV-vis reflectance spectra of samples A–D were measured by diffuse reflectance with the baseline of white magnesium oxide (Fig. 3b). The coating exhibiting the intense blue color (sample B) showed a broadened reflection peak centered around 370 nm (spectrum B in Fig. 3b), whereas such selective reflection was weak for the coating exhibiting the pale blue color (sample A) (spectrum A in Fig. 3b). The references (samples C and D) without the coloration exhibited constant reflectance across the whole visible-light region (spectra C and D in Fig. 3b). Moreover, the blue color of sample B did not change when the photographs were taken with changes in the incident (θ_i) and reflectance (θ_r) angles at $\theta_i = \theta_r$ = 0°, 30°, and 45° (Fig. 3c). The broadened reflectance centered at 370 nm was observed in the UV-vis reflection spectra with changes in the angles ($\theta_i = \theta_r$ = 0°–20°) (Fig. 3d). In this manner, the homogeneous, intense, and noniridescent blue color was obtained by the CN-BA-niobate nanosheets at the optimized coating conditions.

The surface morphology of sample B was flat but uneven (Fig. 3e–h and Fig. S4 in the SI). After the exfoliation and coating, the stacking of the nanosheets on the substrate had d_0 = 2.40 nm, which is smaller than that of the precursor layered CN-BA-niobate (d_0 = 2.98 nm, Fig. 2a). In the layered composites, the guest molecules are intercalated into the interlayer space by exchanging the original ions. The guest molecules interact with each other and self-organize into a specific orientation, such as an interdigitated bilayer state, in the interlayer space. On the other hand, the exfoliated nanosheets are randomly deposited on the substrates without specific guest–guest interaction and orientation in the coating process with the evaporation of the dispersion medium. The corresponding peak was shifted to the wider-angle region and broadened, implying that the tilted angle and conformation of the guests were changed. Based on the image of the laser microscopy, the macroscopic roughness of the coating was a root mean square height (S_q) of 194 ± 8.0 nm (Fig. 3e). The randomly dispersed and stacked nanosheets were observed on the scanning electron microscopy (SEM) image (Fig. 3f). The cross-section viewed from an angle showed the rough surface with variation of the height (Fig. 3g). The average thickness of the thin film was 73.8 ± 13.2 nm on the cross-sectional SEM image (Fig. 3h). When the film thickness (t) is assumed to be in the range of the standard deviation (60.6–87.0 nm), the reflection wavelength (λ) is calculated to be in the range of 279 to 400 nm using (eqn (1)), where the refractive index (n_r) is assumed to be the same as that of niobium oxide (n_r = 2.3).

$$2n_r t = m\lambda \quad (\text{where } m = 1) \tag{1}$$

The range of λ estimated from the thickness is consistent with that observed in the reflection spectrum (Fig. 3b and d).

The reference coating with no structural color (sample C) had the thickness of 726 ± 321 nm and S_q = 364 ± 28 nm (Fig. S4 in the SI). The structural color with the specific reflection in visible light was not observed because of the thick thin film. Another reference film with weak blue color (sample A) had the thickness of 119 ± 47 nm and S_q = 203 ± 57 nm (Fig. S4 in the SI). Compared with sample B, the thicker film with the larger standard deviation leads to a decrease in the reflection in the specific wavelength range. Based on the results, the film thickness is related to the selective reflection (λ) associated with the coloration. The angle independency

originates from an appropriate surface roughness of the thin-film surface. In a previous work, when the domains consisting of the stacked nanosheets are randomly dispersed in the colloidal liquid, the noniridescent color was observed.[37] In the present study, the polydispersity of the film thickness at the microscopic scale corresponds to the randomly dispersed domains, leading to the angle independency of the structural color. In this manner, the noniridescent intense blue color is derived from the thin-film coating with the specific thickness and unevenness.

Effect of the nanosheet sizes on the structural color

The lateral size and thickness of the nanosheets were changed to study their effects on the coating behavior and structural color (Table 1 and Fig. 4). In previous works, the relationship between the coating conditions and morphologies was not fully elucidated because only the successful nanosheet coatings at the limited conditions were used in the published papers. Here, we focused on the effects of the nanosheet sizes on the coating morphology. Table 1 summarizes the nanosheets with the different thickness and lateral-size distribution prepared in the different guest-medium combinations. The API-niobate nanosheets had the larger thickness and narrower lateral-size distribution (Table 1 and Fig. S2 in the SI). The coating exhibited the weaker structural color and inhomogeneous chromaticity (Fig. 4a–c). The surface roughness increased compared with that of the coating by the CN-BA niobate nanosheets (sample B) (Fig. 3e–h and 4b, c). The homogeneous coatings throughout the substrates were not obtained by the nanosheets with the further thicker nanosheets with the narrower lateral-size distribution (Fig. 4d–l). Moreover, the rough surface was observed on the coated area. The results indicate that the thinner nanosheets with the polydispersed lateral size have the potential to achieve the homogeneous coating with the uneven surface. The same results were observed by the other nanosheets in our previous report.[59] The thin and polydispersed nanosheets can fill the gaps in the coating on the substrates. When the defect space is formed on the surface during the spreading of the nanosheets, the flexible thin nanosheets are deposited by conforming to such gaps. In contrast, the plate-like thick nanosheets without such flexibility and conformity are randomly deposited on the surface. In this manner, the thin and polydispersed nanosheets provide the flat coating with the uneven surface exhibiting the noniridescent structural color.

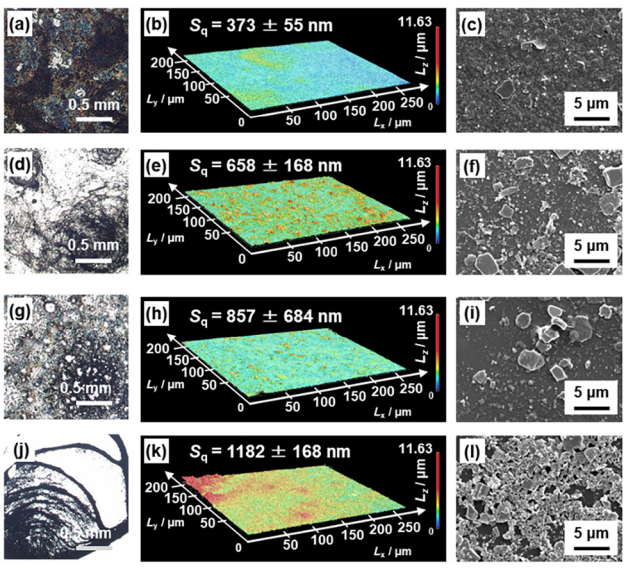

Fig. 4 Optical microscopic (a, d, g and j), laser microscopic (b, e, h and k), and SEM (c, f, j and l) images of the coatings prepared using the nanosheets with different sizes prepared by different guests and dispersion media for the exfoliation (see Table 1). (a–c) API-niobate nanosheets exfoliated in water. (d–f) DAMN-niobate nanosheets exfoliated in water. (g–i) CN-BA-niobate nanosheets exfoliated in ethanol. (j–l) DEA-niobate nanosheets exfoliated in ethanol.

Colorimetric sensing of biogenic amines and their mixtures

The thin film exhibiting the noniridescent structural color is comprised of the multilayered nanosheets. If target guest molecules are introduced or exchanged in the interlayer space, the structural color can be changed by increasing the film thickness coupled with expansion of the interlayer distance. In the present work, the following biogenic amines were used as the targets for the colorimetric sensing (Fig. 5 and Fig. S5 in the SI): histamine (Hst), putrescine (Put), 2-phenylethylamine (Phm), tyramine (Tym), cadaverine (Cad), and γ-aminobutyric acid (Aba).

The sensing was carried out on the nanosheet coatings prepared by drop casting at the optimized conditions, namely C_{ns} = 2.5 g dm^{-3} and V_{ns} = 10 mm^3. The coating was spread over the substrate over an area of *ca.* 2 × 2 mm. An aqueous solution (20 mm^3) containing six amines in the range of 10^{-5}–10^{-2} mol dm^{-3} was dropped on the nanosheet coatings. The coated area exhibiting the structural color was fully covered with the droplet. After evaporation of water, the red-color intensity (x) was calculated from the RGB values of the microscopy image in the selected area of 0.5 × 0.5 mm to estimate the increment (Δx). The changes in the original color were visible at concentrations higher than 10^{-3} mol dm^{-3} for all the amines except Tyr (Fig. 5a, c and Fig. S5 in the SI). Based on the results (Fig. 5 and Fig. S5 in the SI), Δx higher than 0.01 is visually distinguishable. A significant increase in Δx was observed at concentrations higher than 10^{-3} mol dm^{-3} for Hst, Put, Phm, Cad, and Aba and 10^{-4} mol dm^{-3} for Tyr (Fig. 5b, d and Fig. S5 in the SI). The same sensing experiment was performed three times to ensure the reproducibility (N = 3, red squares in Fig. 5b and d). As the reference, the color change with such significant increase in Δx was not observed by dropping purified water without containing the amines (Fig. S8 in the SI). The fact means that the remaining solvent has no effect on the color. In the reproducibility, the errors are caused by the variations in each film because the original color (Δx) is slightly different. If the films with the same thickness and roughness are prepared, the reproducibility can be improved.

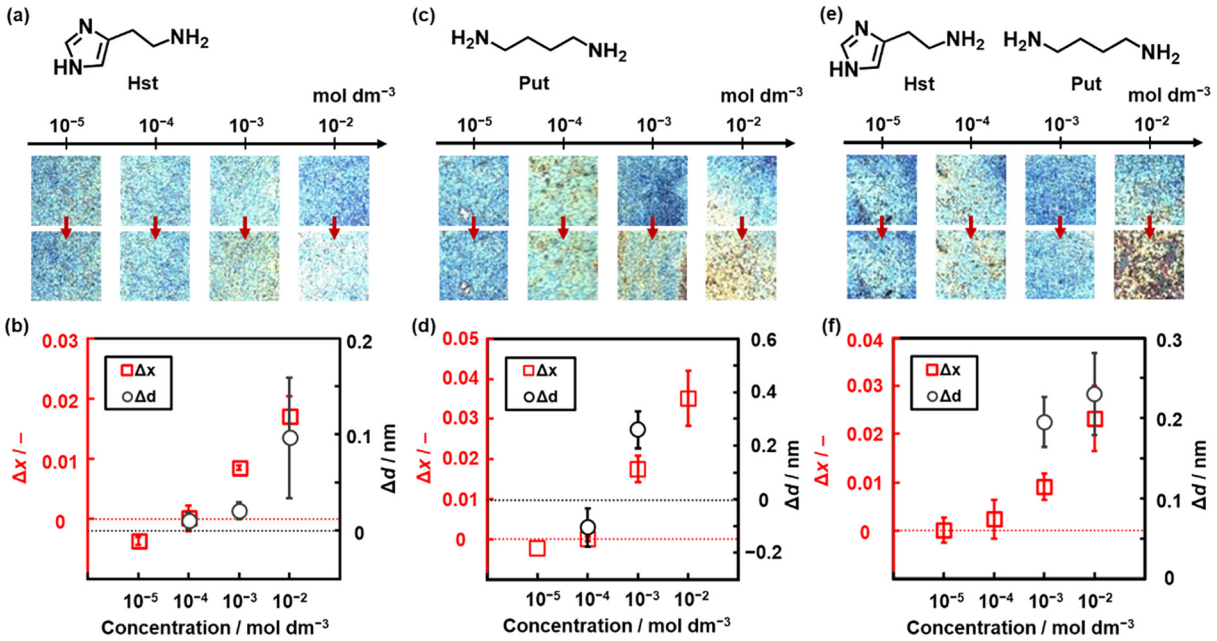

Fig. 5 Colorimetric detection of biogenic amines Hst (a and b) and Put (c and d) and a mixture of Hst and Put (e and f). (a, c and e) Molecular structures and changes in the optical microscopic images before (upper) and after (lower) dropping the aqueous solutions containing the amines. (b, d and f) Relationship between the amine concentration, Δx calculated from the optical microscopic images (left axis), and Δd measured by XRD (right axis).

The peak corresponding to d_0 on the XRD pattern was shifted to the lower angle region with exposure to the amine solution. An increase in d_0 (Δd_0) was observed for the color-changed thin-films with the intercalation of the amines in the interlayer space (N = 3, circles in Fig. 5b, d and Fig. S6 in the SI). The larger Δx and Δd_0 were observed with increasing the concentration of the amines. The next target is the mixture of the biogenic amines (Fig. 5e and f). The mixtures of Hst/Put and Hst/Cad were prepared in the molar ratio of 1 : 1 at the total concentration in the range of 10^{-5}–10^{-2} mol dm^{-3}. The increases in Δx and d_0 were observed by dropping the mixtures at concentrations higher than 10^{-3} mol dm^{-3} (Fig. 5e, f and Fig. S5 and S6 in the SI).

The XRD analyses indicate that an increase in Δx is induced by the intercalation of the target biogenic amines. As the intercalation of the additional guests expands the interlayer space of the multilayered nanosheets, the thickness of the film increases. Therefore, the color changes are induced by varying the reflection wavelength. The larger Δd_0 was observed in the range of 0 to 0.4 nm with increasing the amount of the intercalated amine (Fig. 5b, d, f and Fig. S6 in the SI). As the references, Put and Cad were directly intercalated into the interlayer space of the precursor layered niobate through the ion exchange. In the fully intercalated states, d_0 was 2.99 nm for Phm and 2.15 nm for Cad (Fig. S7 in the SI). These interlayer distances are different from those of the multi-layered CN-BA with the additional intercalation of the guest amines. In the sensing experiment, the biogenic amines as the additional guests are intercalated in the interlayer space with preserving the originally intercalated guests. The affinity between the biogenic amine and the interlayer guest induces the intercalation. When a hexane solution containing 10^{-2} mol dm^{-3} Cad was dropped on the film, the color change was not observed (Fig. S8 in the SI). The affinity of Cad to water and hexane was calculated using the Hansen similarity parameter (HSP) distance. The smaller HSP distance between two compounds means the higher affinity. The HSP distance of Cad was 34.7 for water, 11.6 for hexane, and 7.56 for CN-BA. The calculation implies that Cad has the higher affinity to the interlayer CN-BA compared with that to water. On the other hand, the affinity to hexane is not so different compared with that to CN-BA. The calculation results support that Cad was not intercalated from the hexane solution. The HSP distance of the other biogenic amines to water and hexane showed the similar trend (Table S1 in the SI). Therefore, the multilayered CN-BA niobate nanosheets can accommodate these biogenic amines in the interlayer space from the aqueous solution. In this manner, the color change of the thin film was successfully induced by an increase in the interlayer distance coupled with the intercalation.

Conclusions

The multilayered surface-modified nanosheets were obtained by the exfoliation of the layered composites based on niobate and guest molecules. The coating exhibited the noniridescent structural color on a silicon substrate. The homogeneous

coating with the uneven surface morphology exhibits the non-iridescent structural color. The coating conditions were optimized to enhance the structural color. The thinner nanosheets with the polydispersed lateral size provided the homogeneous coating with the stronger reflection. The multilayered nanosheets in the thin film accommodated the guest molecules as the targets for sensing in the interlayer space. The expansion of the interlayer distance induced the color changes. The harmful biogenic amines and their mixtures in the range of 10^{-3}–10^{-2} mol dm^{-3} were colorimetrically analyzed using the nanosheet thin film. The present work shows the potential of the multilayered nanosheets exhibiting both the anisotropic morphology and intercalation capability.

Conflicts of interest

There are no conflicts to declare.

Data availability

The data supporting this article have been included as part of the supplementary information (SI). Supplementary information: experimental methods, histograms of the nanosheet sizes, microscopy images. Sensing performances. Summary of the related previous works. See DOI: https://doi.org/10.1039/d5nr05285h.

Acknowledgements

This work was partially supported by JST PRESTO (JPMJPR16N2 to Y. O.) and JSPS-KAKENHI (JP22H04559, JP22H02148 to Y. O.).

References

1 M. Osada and T. Sasaki, *Adv. Mater.*, 2012, **24**, 210.
2 V. Nicolosi, M. Chhowalla, M. G. Kanatzidis, M. S. Strano and J. N. Coleman, *Science*, 2013, **340**, 1226419.
3 J. W. Colson and W. R. Dichtel, *Nat. Chem.*, 2013, **5**, 453.
4 M. Pumera, Z. Sofer and A. Ambrosi, *J. Mater. Chem. A*, 2014, **2**, 8981.
5 J. E. ten Elshof, H. Yuan and P. G. Rodriguez, *Adv. Energy Mater.*, 2016, **6**, 1600355.
6 X. Feng and A. D. Schlüter, *Angew. Chem., Int. Ed.*, 2018, **57**, 13748.
7 M. A. Timmerman, R. Xia, P. T. P. Le, Y. Wang and J. E. ten Elshof, *Chem. – Eur. J.*, 2020, **26**, 9084.
8 E. Ruiz-Hitzky and C. Ruiz-Garcia, *Nanoscale*, 2023, **15**, 18959.
9 Y. Wang, Z. Niu, Y. Dai, P. Mu and J. Li, *Nanoscale*, 2023, **15**, 4170.
10 Y. Nishina, *ACS Nano*, 2024, **18**, 332364.
11 Y. He, Y. Zhang, G. Hao, W. Jiang and J. Di, *Nanoscale*, 2024, **16**, 22077.
12 Y. S. Cho and J. Kang, *Nanoscale*, 2024, **16**, 3936.
13 M. Bai, H. Wan, Y. Zhang, S. Chen, C. Lu, X. Liu, G. Chen, N. Zhang and R. Ma, *Chem. Sci.*, 2024, **15**, 16887.
14 K. Ariga, J. Song and K. Kawakami, *Chem. Commun.*, 2024, **60**, 2152.
15 B. Liu, Y. Xia, M. Xie, L. Zhou, G. Vinai, S. A. Morton, A. T. S. Wee, W. G. van der Wiel, W. Zhang and P. K. J. Wong, *Adv. Sci.*, 2024, **11**, 2305277.
16 K. Saito, M. Morita, T. Okada, R. Wijitwongwan and M. Ogawa, *Chem. Soc. Rev.*, 2024, **53**, 10523.
17 M. S. Whittingham, in *Intercalation chemistry*, ed. A. J. Jacobson, Academic Press, New York, 1982.
18 T. E. Mallouk and J. Gavin, *Acc. Chem. Res.*, 1998, **31**, 209.
19 M. Ogawa and K. Kuroda, *Chem. Rev.*, 1995, **95**, 399.
20 E. Ruiz-Hitzky, M. Darder and P. Aranda, *J. Mater. Chem.*, 2005, **15**, 3650.
21 Y. Oaki, *Chem. Commun.*, 2020, **56**, 13069.
22 Q. Wang and D. O'Hare, *Chem. Rev.*, 2012, **112**, 4124.
23 R. Ma and T. Sasaki, *Acc. Chem. Res.*, 2015, **48**, 136.
24 A. Ambrosi and M. Pumera, *Chem. Soc. Rev.*, 2018, **47**, 7213.
25 Y. Oaki, *Chem. Lett.*, 2021, **50**, 305.
26 P. Chavalekvirat, W. Hirunpinyopas, K. Deshsorn, K. Jitapunkul and P. Iamprasertkun, *Precis. Chem.*, 2024, **7**, 300.
27 T. Sasaki, Y. Ebina, T. Tanaka, M. Harada, M. Watanabe and G. Decher, *Chem. Mater.*, 2001, **13**, 4661.
28 M. Osada and T. Sasaki, *J. Mater. Chem.*, 2009, **19**, 2503.
29 A. Usuki, Y. Kojima, M. Kawasumi, A. Okada, Y. Fukushima, T. Kurauchi and O. Kamigaito, *J. Mater. Res.*, 1993, **8**, 1179.
30 T. Lan and T. J. Pinnavaia, *Chem. Mater.*, 1994, **6**, 2216.
31 K. Haraguchi and T. Takehisa, *Adv. Mater.*, 2002, **14**, 1120.
32 P. Ganter and B. V. Lotsch, *Mol. Syst. Des. Eng.*, 2019, **4**, 566.
33 N. Miyamoto and T. Nakato, *Adv. Mater.*, 2002, **14**, 1267.
34 K. Sano, Y. S. Kim, Y. Ishida, Y. Ebina, T. Sasaki, T. Hikima and T. Aida, *Nat. Commun.*, 2016, **7**, 12559.
35 E. Mouri, C. Ogami, T. Fukumoto and T. Nakato, *Chem. Lett.*, 2020, **49**, 717.
36 W. Yang, S. Yamamoto, K. Sueyoshi, T. Inadomi, R. Kato and N. Miyamoto, *Angew. Chem., Int. Ed.*, 2021, **60**, 8466.
37 N. Miyamoto and S. Yamamoto, *ACS Omega*, 2022, **7**, 6070.
38 K. Szendrei-Ternesi, A. Jiménez-Solano and B. V. Lotsch, *Adv. Mater.*, 2018, **30**, 1803730.
39 P. Ganter, L. M. Schoop, M. Dantl and B. V. Lotsch, *Chem. Mater.*, 2018, **30**, 2557.
40 Y. X. Yan, H. B. Yao, L. B. Moo, A. M. Asiri, K. A. Alamry, H. M. Marwani and S. H. Yu, *Small*, 2016, **12**, 745.
41 H. Chi, Z. Xu, X. Duan, J. Yang, F. Wang and Z. Li, *ACS Appl. Mater. Interfaces*, 2019, **11**, 32390.
42 C. Cheng, X. Zhang, M. Li, D. Pei, Y. Chen, X. Zhao and C. Li, *J. Colloid Interface Sci.*, 2022, **617**, 604.
43 E. Colusso, G. Perotto, Y. Wang, M. Sturaro, F. Omenetto and A. Martucci, *J. Mater. Chem. C*, 2017, **5**, 3924.

44 M. Kohri, Y. Nannichi, T. Taniguchi and K. Kishikawa, *J. Mater. Chem. C*, 2015, **3**, 720.
45 Y. Takeoka, *Chem. Commun.*, 2018, **54**, 4905.
46 N. Kumano, H. Tanaka, Y. Akimoto and H. Nakamura, *J. Mater. Chem. C*, 2020, **8**, 16749.
47 F. Wang, J. Wang, P. Gao, Y. Wang, W. Ma, Z. Zhang, X. Men and Y. Lu, *ACS Appl. Nano Mater.*, 2023, **6**, 16555.
48 Y. Haraguchi, H. Imai and Y. Oaki, *Adv. Mater. Interfaces*, 2022, **25**, 2201111.
49 Y. Oaki, *Chem. Lett.*, 2021, **50**, 305.
50 M. Honda, Y. Oaki and H. Imai, *Chem. Mater.*, 2014, **26**, 3579.
51 G. Nakada, H. Imai and Y. Oaki, *Chem. Commun.*, 2018, **54**, 244.
52 R. Mizuguchi, Y. Igarashi, H. Imai and Y. Oaki, *Nanoscale*, 2021, **13**, 3853.
53 Y. Haraguchi, Y. Igarashi, H. Imai and Y. Oaki, *Adv. Theory Simul.*, 2021, **4**, 2100158.
54 R. Hikichi, Y. Tokura, Y. Igarashi, H. Imai and Y. Oaki, *Bull. Chem. Soc. Jpn.*, 2023, **96**, 766.
55 Y. Haraguchi, H. Imai and Y. Oaki, *iScience*, 2022, **25**, 104933.
56 N. Kaur, S. Chopra, G. Singh, P. Raj, A. Bhasin, S. K. Sahoo, A. Kuwar and N. Singh, *J. Mater. Chem. B*, 2018, **6**, 4872.
57 A. I. Danchuk, N. S. Komova, S. N. Mobarez, S. Y. Doronin, N. A. Burmistrova, A. V. Markin and A. Duerkop, *Anal. Bioanal. Chem.*, 2020, **412**, 4023.
58 M. J. Grant, K. M. Wolfe, C. R. Harding and G. C. Welch, *J. Mater. Chem. C*, 2023, **11**, 9749.
59 H. Sudo, Y. Nishina, H. Imai and Y. Oaki, *Nanoscale*, 2025, **17**, 27362.